NASA TECHNICAL NOTE

NASA TN D-8221

ANALYSIS AND DESIGN OF A CANTILEVER-MOUNTED RESILIENT-PAD GAS-LUBRICATED THRUST BEARING

Izhak Etsion

Lewis Research Center
Cleveland, Ohio 44135

NATIONAL AERONAUTICS AND SPACE ADMINISTRATION • WASHINGTON, D. C. • MAY 1976

1. Report No. NASA TN D-8221	2. Government Accession No.	3. Recipient's Catalog No.
4. Title and Subtitle ANALYSIS AND DESIGN OF A CANTILEVER-MOUNTED RESILIENT-PAD GAS-LUBRICATED THRUST BEARING		5. Report Date May 1976 6. Performing Organization Code
7. Author(s) Izhak Etsion		8. Performing Organization Report No. E-8667
9. Performing Organization Name and Address Lewis Research Center National Aeronautics and Space Administration Cleveland, Ohio 44135		10. Work Unit No. 505-04 11. Contract or Grant No.
12. Sponsoring Agency Name and Address National Aeronautics and Space Administration Washington, D.C. 20546		13. Type of Report and Period Covered Technical Note 14. Sponsoring Agency Code
15. Supplementary Notes		

16. Abstract

A thrust bearing consisting of pads mounted on resilient, metallic, cantilever beams is described and analyzed. Compliance and stiffness of the bearing assembly are discussed, and the effects of bearing design parameters on performance are shown. After the general analysis, a design example is presented for a flat sector-shaped gas bearing. A special case where zero axial movement of the runner can be obtained is pointed out.

17. Key Words (Suggested by Author(s)) Bearings Gas bearings Thrust bearings Compliant bearings	18. Distribution Statement Unclassified - unlimited STAR category 37		
19. Security Classif. (of this report) Unclassified	20. Security Classif. (of this page) Unclassified	21. No. of Pages 22	22. Price* $3.50

* For sale by the National Technical Information Service, Springfield, Virginia 22161

ANALYSIS AND DESIGN OF A CANTILEVER-MOUNTED RESILIENT-PAD GAS-LUBRICATED THRUST BEARING

by Izhak Etsion*

Lewis Research Center

SUMMARY

A thrust bearing consisting of pads mounted on resilient, metallic, cantilever beams is described and analyzed. Compliance and stiffness of the bearing assembly are discussed, and the effects of bearing design parameters on performance are shown. After the general analysis, a design example is presented for a flat sector-shaped gas bearing. A special case where zero axial movement of the runner can be obtained is pointed out.

INTRODUCTION

Many modern gas-bearing applications require tolerance to dirt ingestion and high-temperature operating capability. The first requirement was met by the development of bearings with flexible or compliant geometry. These are the foil bearings and the compliant surface or compliant mounted bearings. In reference 1 the various designs are briefly summarized and their main disadvantages pointed out. The foil bearings are less successful as thrust bearings than as journal bearings. Compliant bearings that use elastomeric materials are temperature limited. Also in reference 1 a new type of bearing is described. This is a resilient-pad thrust bearing that does not contain any elastomers in the bearing assembly. It consists of sector-shaped flat pads mounted asymmetrically on resilient foil annular beams. This combines compliance with high-temperature operating capability.

---

*National Research Council - National Aeronautics and Space Administration Research Associate.

The bearing analysis in reference 1 was simplified by assuming rectangular pads and treating the bearing as a slider with constant velocity. The annular support was approximated by rectangular beams.

In the course of experimental work being done at NASA Lewis Research Center it was found that the analysis of reference 1 was oversimplified and the bearing failed to function under moderate and high loads. Hence a better analysis is needed. As a first step the actual flat-pad sector-shaped gas bearing was analyzed (ref. 2) by taking into account both pitch and roll of the pad; and results for load capacity, power loss, and center-of-pressure location were obtained.

It is shown in reference 2 that the load capacity of a flat sector-shaped pad is maximized whenever the pad tilt results in a uniformly minimum film thickness along its trailing edge. For that reason and to get better control of the support characteristics, the annular beams of reference 1 are replaced in this report by straight cantilever beams. The bearing concept analyzed thus consists of a sector-shaped flat pad mounted on a rectangular cantilever beam, as shown in figures 1 and 2.

ANALYSIS

Cantilever Design

The sector-shaped pad is attached to the cantilever beam along a line parallel to the pad trailing edge and at a distance D from that edge (fig. 2). This line serves as a pivot about which the pad is tilted. As is shown in reference 2 a pure pitch about some radial line is equivalent to combined pitch and roll about a given point. It is also shown in reference 2 that the radial pivot line that will maximize the load capacity of the bearing is its trailing edge. This is also true for any pivot line parallel to the trailing edge. The pitch γ about the pivot line, the distance D, and the film thickness h_2 along the trailing edge completely describe the pad orientation. (All symbols are defined in the appendix.)

The load W acting on the pad at the center of pressure causes a deflection of the cantilever beam, as shown in figure 2. From the strength of materials (e.g., ref. 3) the formulas for the deflection and angle of the end of a cantilever due to a force W and a moment M are

$$\delta_b = W \frac{l^3}{3EI} + M \frac{l^2}{2EI} \tag{1a}$$

$$\gamma = W\frac{l^2}{2EI} + M\frac{l}{EI} \tag{1b}$$

where $M = W(x_{cp} - D)$ is clockwise for $x_{cp} < D$ and

$$x_{cp} = r_{cp}\sin(\beta - \theta_{cp}) \tag{2}$$

Substituting the expression for M into equations (1) yields

$$\delta_b = \frac{Wl^3}{2EI}\left(\frac{2}{3} + \frac{x_{cp} - D}{l}\right) \tag{3a}$$

$$\gamma = \frac{Wl^2}{2EI}\left(1 + 2\,\frac{x_{cp} - D}{l}\right) \tag{3b}$$

To function properly, the pad must be tilted so that both δ_b and γ will be positive. In the case where the center of pressure is behind the pivot line, $x_{cp} - D < 0$. This immediately imposes the demand of

$$l > 2(D - x_{cp}) \tag{4}$$

Before startup, if the pad is loaded, the deflection characteristic should be such that the runner touches the pad only at its trailing edge. This provides the wedge-shaped film needed for lift-off. In that case the load acts at a distance $x_{cp} = 0$, and condition (4) becomes

$$l > 2D \tag{5}$$

Runner Axial Displacement

The axial displacement of the runner as a function of load and speed is an important parameter in many applications where tight tolerances are necessary. We assume that under zero load and speed the pad surface is in contact with the runner and that the beam remains undeflected. The runner displacement δ_r under a load W at any speed is

$$\delta_r = \delta_b \llcorner h_p \tag{6}$$

where h_p, the film thickness along the pivot line, is simply

$$h_p = h_2 + \gamma D \tag{7}$$

Hence

$$\delta_r = \delta_b - \gamma D - h_2 \tag{8}$$

For nonresilient geometries, such as fixed pads or rigidly supported tilting pads, $\delta_b = 0$; and at any nonzero load, $h_p > 0$. Hence it is clear from equation (6) that $\delta_r = -h_p$ and the runner is displaced from its zero-load, zero-speed position. For flexible support, however, $\delta_b \neq 0$ and δ_r can be controlled by the beam design.

Rearranging equation (8) gives the beam deflection

$$\delta_b = \delta_r + \gamma D + h_2 \tag{9}$$

Substituting equation (9) into (3a) and dividing by (3b) yields

$$\frac{\delta_r + h_2}{\gamma} + D = l \frac{\frac{2}{3} + \frac{x_{cp} - D}{l}}{1 + \frac{2(x_{cp} - D)}{l}} \tag{10}$$

or after algebraic manipulations

$$\alpha = \frac{1}{3} \frac{l}{x_{cp}} \left[1 + \frac{\frac{l}{x_{cp}} + 1 - \frac{D}{x_{cp}}}{\frac{l}{x_{cp}} + 2\left(1 - \frac{D}{x_{cp}}\right)} \right] - \frac{D}{x_{cp}} \tag{11}$$

where α is a dimensionless parameter defined as

$$\alpha = \frac{\frac{\delta_r}{h_2} + 1}{\frac{\gamma r_o}{h_2} \frac{x_{cp}}{r_o}}$$

Selecting values for D/x_{cp} and l/x_{cp} and keeping condition (5), which is $l/x_{cp} >$

$2D/x_{cp}$, give by equation (11) the corresponding value for α. Hence the dimensionless runner axial displacement δ_r/h_2 is found from

$$\frac{\delta_r}{h_2} = \alpha \frac{\gamma r_o}{h_2} \frac{x_{cp}}{r_o} - 1 \tag{12}$$

In a fixed-geometry thrust bearing the loaded runner at zero speed touches the pad along the trailing edge. When lift-off occurs the runner moves a distance h_2 back from its zero-speed position and against the load direction, and thus, $\delta_r/h_2 = -1$. In a tilting pad bearing, where the pivots are rigidly supported, the back movement of the loaded runner due to its velocity must also accommodate the tilt of the pad, and hence $\delta_r/h_2 < -1$. In bearings having compliant support, this backward movement is compensated by the support deflection, and $\delta_r/h_2 > -1$. Thus, the nondimensional parameter α in equation (12) indicates the amount of compliance of the bearing, ranging from zero for rigidly supported fixed pads to any amount of compliance as α becomes larger than zero.

With α as a compliance parameter, it is instructive to examine equation (11) before any selection of dimensions l and D is made. In practical design, the beam portion extending beyond the trailing edge is limited by the space available for the bearing housing. Therefore, the dimension $(l - D)$ rather than the total length l (fig. 2) has to be kept within limits. Rearranging equation (11) in terms of $(l - D)/x_{cp}$ and D/x_{cp} we have

$$\alpha = \frac{1}{3}\left(\frac{l - D}{x_{cp}} + \frac{D}{x_{cp}}\right)\left(1 + \frac{\frac{l - D}{x_{cp}} + 1}{\frac{l - D}{x_{cp}} + 2 - \frac{D}{x_{cp}}}\right) - \frac{D}{x_{cp}} \tag{13}$$

Keeping $(l - D)/x_{cp}$ constant and differentiating α with respect to the variable D/x_{cp} clearly shows that α has a minimum when $D/x_{cp} = 1$. Also, from equation (13) it is seen that, for values of D/x_{cp} close to unity, α is well approximated by

$$\alpha = \frac{2}{3}\frac{l - D}{x_{cp}} - \frac{1}{3}\frac{D}{x_{cp}}$$

and is affected less and less by D/x_{cp} as $(l - D)/x_{cp}$ becomes larger than 1.

Figure 3 presents values of the compliance parameter α as a function of pivot location D/x_{cp} at various values of $(l - D)/x_{cp}$, as well as the loci of $l = 2D$ and

$l = 0$. It should be recalled that the condition for self-startup given by (5) is $l > 2D$. Hence practical values of α are confined to the region between these two loci. As will be shown in a design example, the clearance parameter $\gamma r_o/h_2$, the minimum film thickness h_2, and the center-of-pressure location x_{cp}/r_o are known at any given design point. Hence for any desired δ_r a proper value of α can be selected by equation (12). It is also clear from equation (12) that a special design is possible where $\delta_r = 0$. Such a design might be advantageous in some applications and is unique to compliant bearings. For zero axial movement of the runner at the design point we have from equation (12)

$$\alpha = \left(\frac{\gamma r_o}{h_2} \frac{x_{cp}}{r_o} \right)^{-1}$$

In general, higher values of α are preferred in order to achieve more compliance. The maximum compliance is limited, however, by the space in the bearing housing and by the acceptable axial displacement of the shaft.

Bearing Axial Stiffness

Another parameter that is of importance in bearing design is the overall axial stiffness K. It can be easily shown that in a compliant mounted multipad bearing, low stiffness is associated with better load sharing among the pads. In case of any misalinement of the runner, the out-of-balance exciting force on an individual pad is reduced and the bearing stability might be improved.

Referring to the bearing "softness" as the inverse of its stiffness we have

$$\frac{1}{K} = \frac{d(\delta_r)}{d(W_t)} = \frac{d(\delta_r)}{n\, d(W)}$$

The axial displacement of the runner δ_r depends on the variation in h_2 and the axial movement of the pad trailing edge. Substituting equation (8) for δ_r we have

$$\frac{n}{K} = \frac{d(\delta_b)}{d(W)} - D\frac{d(\gamma)}{d(W)} - \frac{d(h_2)}{d(W)} \tag{14}$$

Since the last term on the right side of equation (14), namely $d(h_2)/d(W)$, is always negative, it is the other terms, describing the change in the trailing-edge displace-

ment, that determine the magnitude of the stiffness. The higher the change in that displacement, the softer the bearing.

The terms "softness" and "compliance parameter," which are used in this report, describe two different features of the bearing. The compliance parameter is related to the net axial displacement of a loaded runner due to change in its speed from zero to the design value. The softness, or stiffness, is related to an incremental change in the displacement due to a change in the load at a constant speed.

Denoting the trailing-edge displacement by δ_t we have

$$\frac{d(\delta_t)}{d(W)} = \frac{d(\delta_b)}{d(W)} - D\frac{d(\gamma)}{d(W)} \tag{15}$$

Differentiating equations (3a) and (3b) with respect to W and substituting into equation (15) yields

$$2EI\frac{d(\delta_t)}{d(W)} = l^3\left(\frac{2}{3} + \frac{x_{cp} - D}{l}\right) - Dl^2\left(1 + 2\frac{x_{cp} - D}{l}\right) \tag{16}$$

Again after rearranging in terms of $l - D$ rather than l and dividing by x_{cp}^3, equation (16) becomes

$$\frac{2EI}{x_{cp}^3}\frac{d(\delta_t)}{d(W)} = \frac{2}{3}\left(\frac{D}{x_{cp}}\right)^3 - \left(\frac{D}{x_{cp}}\right)^2 + \frac{2}{3}\left(\frac{l - D}{x_{cp}}\right)^3 + \left(\frac{l - D}{x_{cp}}\right)^2 \tag{17}$$

Maintaining $(l - D)/x_{cp}$ constant and differentiating equation (17) with respect to D/x_{cp} yields a maximum for $d(\delta_t)/d(W)$ at $D/x_{cp} = 0$ and a minimum at $D/x_{cp} = 1$.

In practice, $l - D$ must be larger than D (see condition (5)) and can be three or four times larger. In that case it is clear from equation (17) that the effect of D on the bearing stiffness is negligible compared with that of $l - D$. The same result is concluded from equation (13) in regard to the compliance parameter α (see also fig. 3). Hence the accurate location D of the pivot line is not crucial, leaving much flexibility for manufacturing tolerances.

So far nothing has been specified regarding the nature of the lubricant or the clearance shape. Therefore, the preceding analysis is valid for both compressible and incompressible hydrodynamic bearings of flat, stepped, crowned, or any other pad surface form. Moreover, not only sector-shaped pads, but also rectangular sliders can be used as the load-carrying members.

To avoid unnecessary torsional moments, the radial or transverse location of the

cantilever beam should be such that the beam centerline is perpendicular to the pad trailing edge and passes through the center of pressure.

DESIGN EXAMPLE

As an example of the procedure described, a six-pad gas-lubricated bearing having the following dimensions and operating conditions was chosen:

Outer radius of pad, r_o, cm	5
Inner radius of pad, r_i, cm	2.5
Angular extent of pad, β, deg	45
Ambient pressure, p_a, N/m^2	1×10^5
Dynamic viscosity of gas, μ, $N\text{-}sec/m^2$	1.86×10^{-5}
Shaft speed, ω, rpm	34 000
Total load, W_t, N	74
Young's modulus of beam material, E, N/m^2	2.1×10^{11}

The first step is to determine the design parameters for optimum operation, which means the highest value for the minimum film thickness at the design load. Since h_2 appears in the denominator in the definition of the compressibility number Λ (see appendix), the highest value for h_2 is achieved when the bearing is operated at the lowest possible Λ. This corresponds to a curve for constant Λ in the design chart, figure 4 (from ref. 2), which gives the design load at its extrema. The values of those extrema, along with the corresponding optimum clearance parameters, are plotted against Λ in figure 5.

In the present design the unit load W_t/np_aA is 0.166, which corresponds to the maximum unit load at $\Lambda = 50$. From the optimum Λ and the design speed ω, h_2 is obtained. The optimum value of the clearance parameter is also found from figure 5; thus, the beam slope γ is determined. Also x_{cp} is found at the design point from figure 6, which is crossplotted from the information on center-of-pressure location given in reference 2.

In our example, for $\Lambda = 50$ and $\omega = 34\ 000$ rpm, the minimum film thickness h_2 is 1.4×10^{-3} centimeter. From figures 5 and 6, at the design point, $\gamma r_o/h_2 = 3.2$ and $x_{cp}/r_o = 0.2$; hence, $x_{cp} = 1$ centimeter. A value of $(\ell - D)/x_{cp} = 4$ was selected because of space limitation, and a value of $D/x_{cp} = 0$ was chosen to achieve low stiffness. From equation (13), α is 2.45; from equation (12), δ_r/h_2 is 0.6; and from equation (3b), the beam moment of inertia I is 7.75×10^{-3} cm^4. A beam width b of 2 centimeters was selected, resulting in a beam thickness t of 3.6 millimeters.

From reference 2 the radial location of the center of pressure r_{cp}/r_o is 0.767, which determines the radial location of the beam.

Operating Characteristics at Various Loads and Speeds

After designing a bearing for optimum operation at a given speed and load, it is necessary to determine its operating characteristics over a range of operating speeds and loads.

For a given value of W_t the intercepts of the dimensionless pad load $W/\Lambda p_a A$ with curves of constant Λ such as those of figure 4 are determined. For each intercept a value of $\gamma r_o/h_2$ is obtained. Values of x_{cp}/r_o are obtained from curves such as those in figure 6. From equation (3b) the beam slope γ is calculated and h_2 is obtained. A value of ω at each intercept point in figure 4 can then be calculated. At each such point the values of $(\ell - D)/x_{cp}$ and D/x_{cp} are determined from the selected dimensions ℓ and D, and the nondimensional parameter α is obtained from equation (13). Then values of δ_r/h_2 are calculated by equation (12), and the runner axial displacement δ_r is found. Figure 7 shows a plot of minimum film thickness as a function of shaft speed for the present beam design at two total loads. Figure 8 shows the runner axial displacement as a function of shaft speed at various total loads.

Before startup, if the pad is loaded, the deflection characteristics are such that the runner touches the pad at its trailing edge and $\gamma r_o/h_2$ is infinite. When the runner starts to rotate, lift-off occurs and h_2 increases with speed. At zero speed the runner, under the load, is displaced from its zero-load position and follows the deflected beam. However, as the speed increases the runner is lifted back towards its zero-load position. And as the speed continues to increase, the runner passes the zero-load position.

The bearing stiffness K at any given speed and load can be easily found from figure 8. This is done by crossplotting W_t against δ_r for the given speed and finding the slope $d(W_t)/d(\delta_r)$ at the given load. In figure 9 such variation of δ_r with W_t is shown for various shaft speeds. The bearing stiffness is constant over a wide range of operating conditions.

In many practical applications the load on the bearing varies with speed. If this variation is known, the corresponding points can be plotted in figure 8 to describe the runner axial movement. A particular case is the line $\delta_r = 0$. As was mentioned, a special design where δ_r is zero at the design point can be performed by choosing a proper compliance parameter α. However, if for such a bearing the off-design load can be controlled and related to the speed in order to result in that particular locus, a unique design can be accomplished where the runner never moves axially from its

zero-speed, zero-load position.

The friction torque F/ω at each point is calculated from the information contained in figure 10 (from ref. 2). At each intercept point in figure 4 the values of W, Λ, and $\gamma r_o/h_2$ are known. Hence from figure 10 the corresponding values of $F/W\omega h_2$ are obtained. The values of ω and h_2 that were already calculated are now used to obtain the power loss F or the friction torque F/ω. In figure 11 the torque is plotted against shaft speed at two different loads.

Summary of Beam Design Procedure

The beam design procedure can be summarized as follows:

(1) For a given load W_t and a given bearing geometry, determine the pad unit loading W/p_aA, where $W = W_t/n$ and $A = \beta\left(r_o^2 - r_i^2\right)/2$.

(2) From curves such as figure 5, determine the optimum Λ and the optimum clearance parameter $\gamma r_o/h_2$.

(3) Calculate h_2 at the design speed ω from $h_2 = \left(6\mu\omega r_o^2/p_a\Lambda\right)^{1/2}$ and use this value to calculate the pad tilt γ from the optimum clearance parameter.

(4) From curves such as figure 6 determine x_{cp} at the design point.

(5) Considering space limitation, select l - D and choose D. (A value of $D/x_{cp} = 0$ will result in the lowest stiffness.) Use equation (11) to determine the compliance parameter α and calculate the runner axial displacement from $\delta_r = \alpha\gamma x_{cp} - h_2$. Check if this displacement is acceptable and alter $(l - D)/x_{cp}$ accordingly to obtain other values for α and δ_r. The term $(l - D)/x_{cp}$ is mostly limited by the available space in the bearing housing and not by the runner displacement.

(6) With the final values of l and D, use equation (3b) to calculate the beam moment of inertia I. Select a value for the beam width b and calculate its thickness t from $(12\ I/b)^{1/3}$.

A flow diagram summarizing the beam design procedure is presented in figure 12. Another diagram for off-design calculation is given in figure 13.

SUMMARY OF RESULTS

The procedure for optimizing the design of a cantilever-mounted, resilient-pad, gas-lubricated thrust bearing for operation at a given load and speed was shown to be straightforward. A compliance parameter was defined that determines the axial displacement of the runner and indicates the bearing compliance compared with rigid

configurations. The operating characteristics of an optimized bearing design were determined for a range of operating speeds and loads in a design example. And a way to calculate bearing stiffness was described. The effect of cantilever beam dimensions on bearing characteristics was discussed, and it was concluded that bearing compliancy and stiffness are mostly affected by the length of that portion of the beam that extends beyond the pad trailing edge. Increasing this length increases the compliance and reduces the stiffness. It was also shown that a special thrust bearing can be designed where the runner axial movement is zero, provided off-design loads can be controlled.

Lewis Research Center,
National Aeronautics and Space Administration,
Cleveland, Ohio, March 31, 1976,
505-04.

APPENDIX - SYMBOLS

A	pad area, $\beta\left(r_o^2 - r_i^2\right)/2$
b	beam width
D	distance of pivot line from trailing edge (positive if pivot line is ahead of trailing edge)
E	Young's modulus of beam material
F	power loss
h_p	film thickness along pivot line
h_2	minimum film thickness
I	moment of inertia of flexible beam, $bt^3/12$
K	bearing axial stiffness
l	length of beam
M	moment acting on beam end
n	number of pads
p_a	ambient pressure
r_{cp}	radial center-of-pressure location
r_i	pad inner radius
r_o	pad outer radius
t	thickness of flexible beam
W	pad loading, W_t/n
W_t	total load
x_{cp}	distance of center of pressure from trailing edge
α	compliance parameter, $\left(\frac{\delta_r}{h_2} + 1\right) \Big/ \frac{\gamma r_o}{h_2} \frac{x_{cp}}{r_o}$
β	angular extent of pad
γ	slope at beam free end, equal to pad tilt about its pivot line
δ_b	deflection of flexible beam
δ_r	axial displacement of runner, in direction of load

δ_t axial displacement of pad trailing edge, in direction of load, $\delta_b - \gamma D$

θ_{cp} angular center-of-pressure location, measured from pad leading edge

Λ compressibility number, $6\mu\omega r_o^2/p_a h_2^2$

μ dynamic viscosity

ω shaft speed

REFERENCES

1. Anderson, W. J.: Analysis of an All-Metallic Resilient Pad Gas Lubricated Thrust Bearing. J. Lub. Technol., ASME Trans., vol. 97, no. 2, Apr. 1975, pp. 296-302.

2. Etsion, Izhak: Analysis of the Gas-Lubricated Flat-Sector-Pad Thrust Bearing. NASA TN D-8220, 1976.

3. Roark, Raymond J.: Formulas for Stress and Strain. McGraw-Hill Book Co., Inc., 1965.

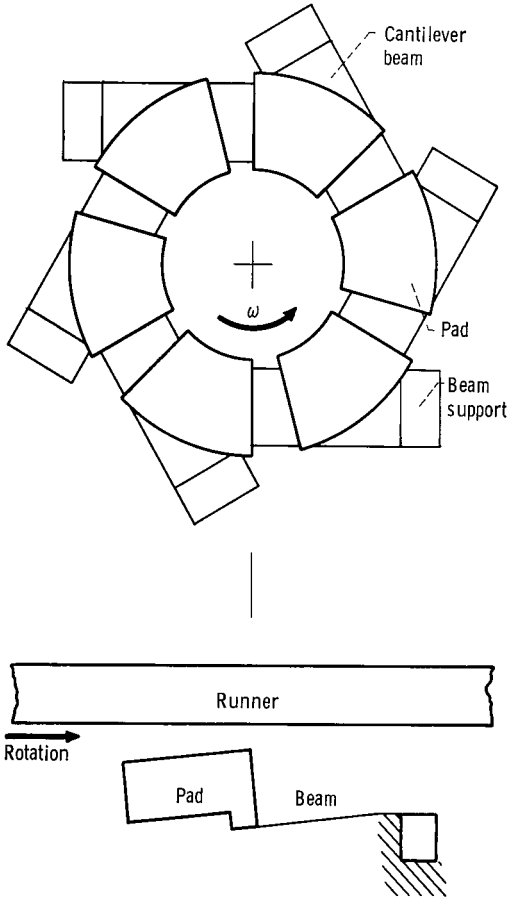

Figure 1. - Cantilever-mounted multipad bearing.

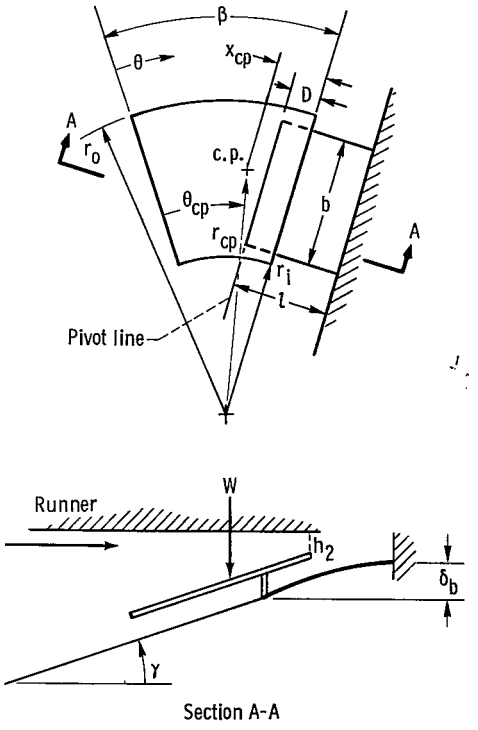

Figure 2. - Individual pad and beam.

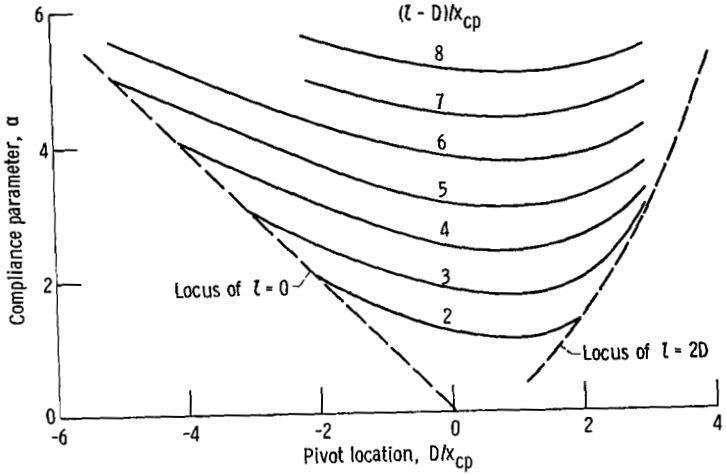

Figure 3. - Compliance parameter as function of pivot location at various $(\ell - D)/x_{cp}$ ratios.

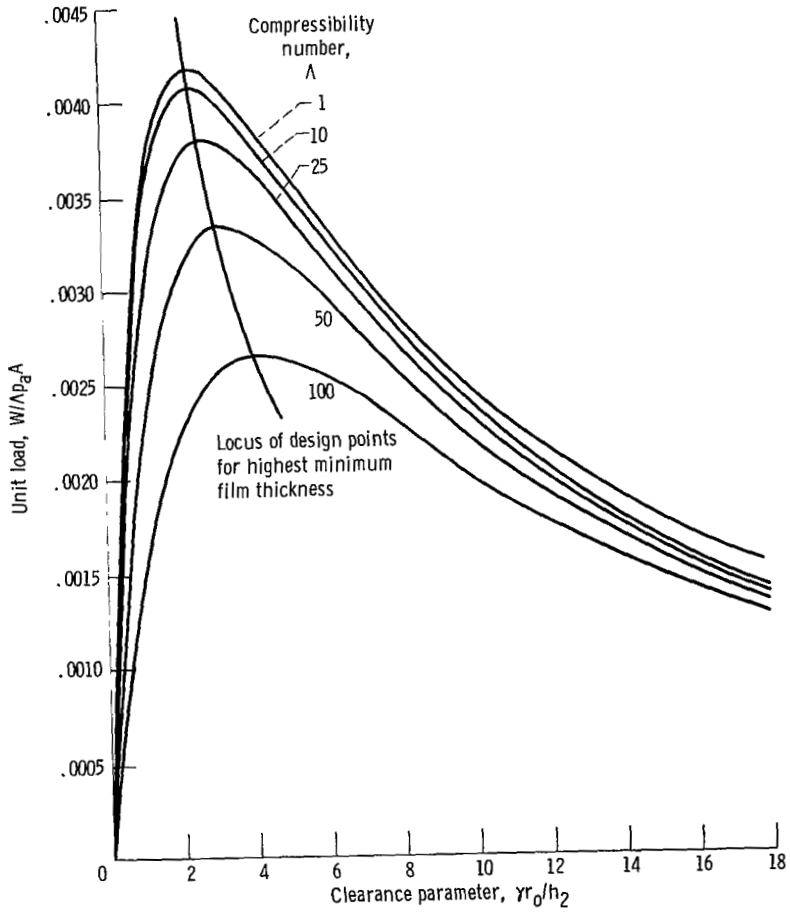

Figure 4. - Load as function of clearance parameter at various compressibility numbers. Ratio of inner to outer pad radius, r_i/r_o, 0.5; angular extent of pad, β, 45^0. (From ref. 2.)

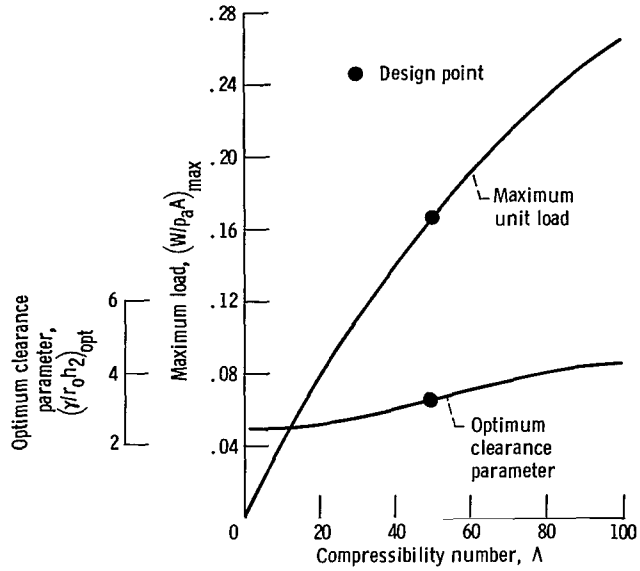

Figure 5. - Maximum available unit load and optimum clearance parameter as functions of compressibility number. Ratio of inner to outer pad radius, r_i/r_o, 0.5; angular extent of pad, β, 45°.

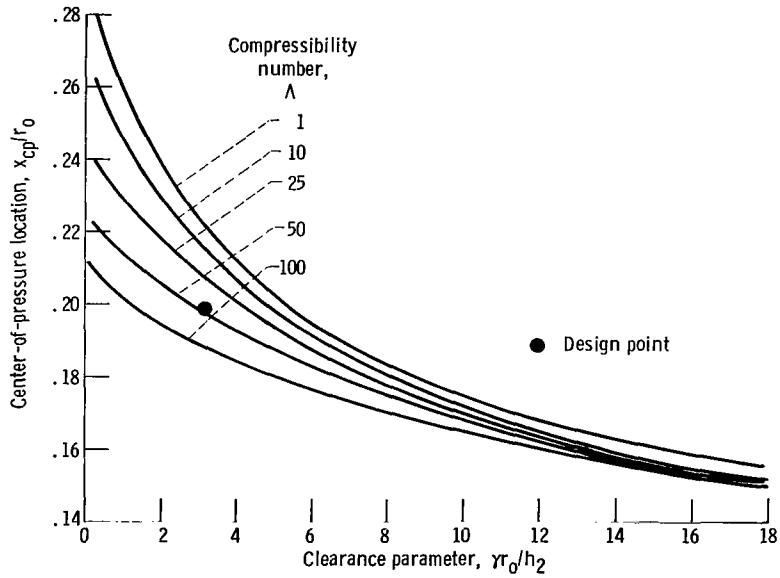

Figure 6. - Center-of-pressure distance from trailing edge as function of clearance parameter at various compressibility numbers. Ratio of inner to outer pad radius, r_i/r_o, 0.5; angular extent of pad, β, 45°.

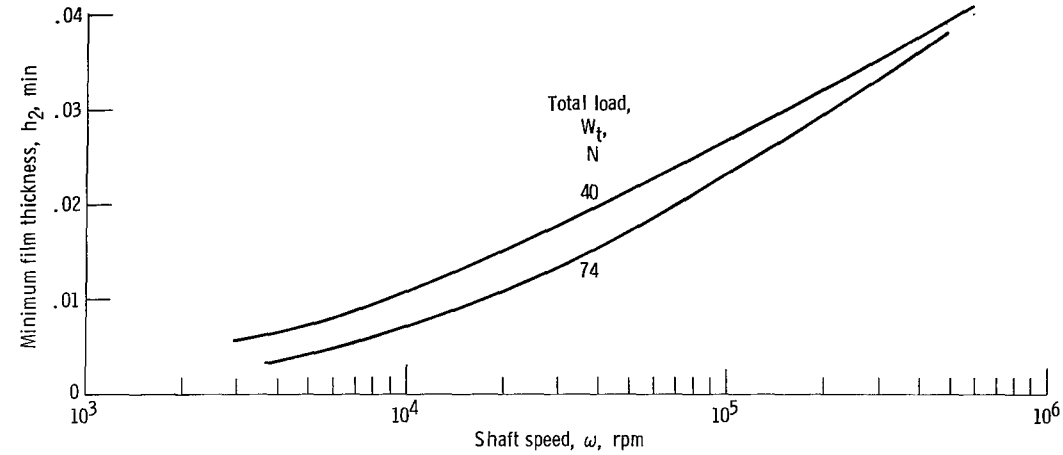

Figure 7. - Minimum film thickness as function of shaft speed. Length of beam, ℓ, 4 centimeters; pivot location, D, 0; moment of inertia, I, 7.75×10^{-3} cm^4.

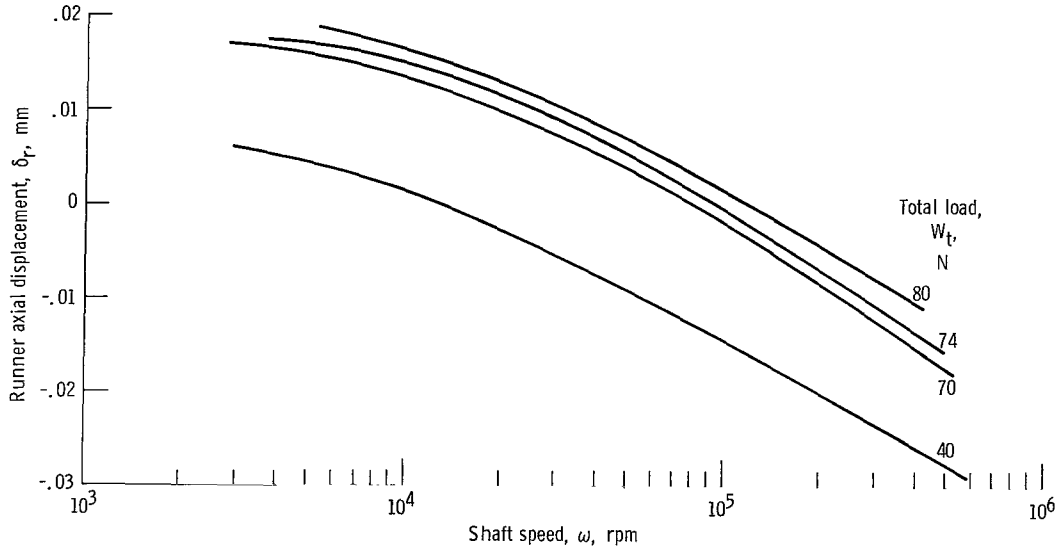

Figure 8. - Runner axial displacement as function of shaft speed at various loads. Length of beam, ℓ, 4 centimeters; pivot location, D, 0; moment of inertia, I, 7.75×10^{-3} cm^4.

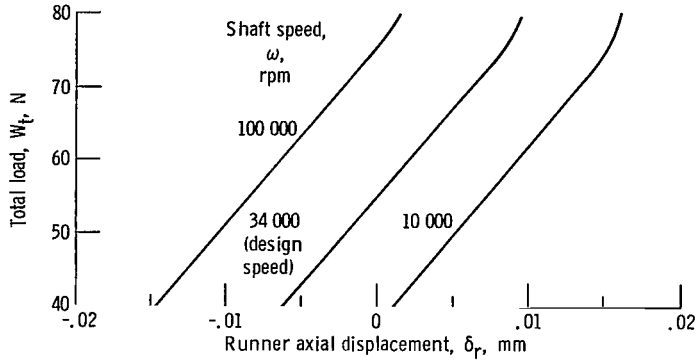

Figure 9. - Runner axial displacement as function of total load for various shaft speeds. Length of beam, ℓ, 4 centimeters; pivot location, D, 0; moment of inertia, I, 7.75×10^{-3} cm^4.

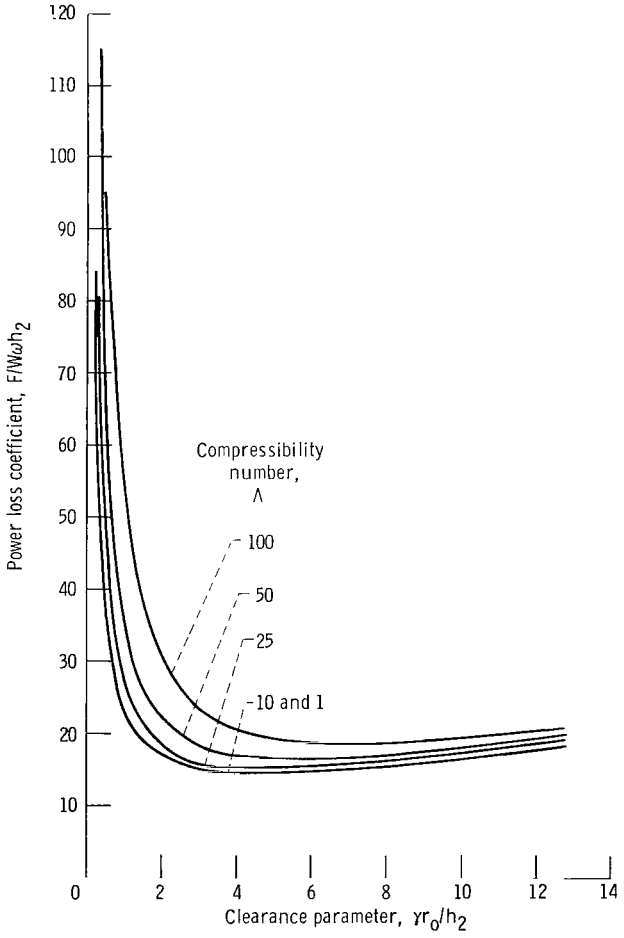

Figure 10. - Power loss coefficient as function of clearance parameter at various compressibility numbers. Ratio of inner to outer pad radius, r_i/r_o, 0.5; angular extent of pad, β, 45^o. (From ref. 2.)

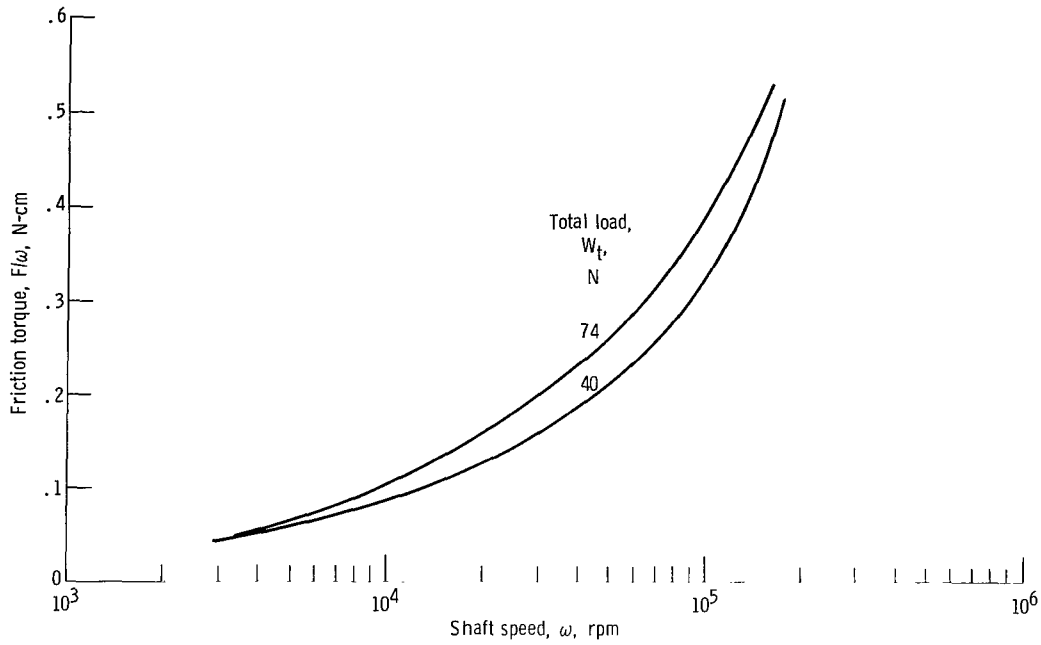

Figure 11. - Friction torque as function of shaft speed. Length of beam, l, 4 centimeters; pivot location, D, 0; moment of inertia, I, 7.75×10^{-3} cm^4.

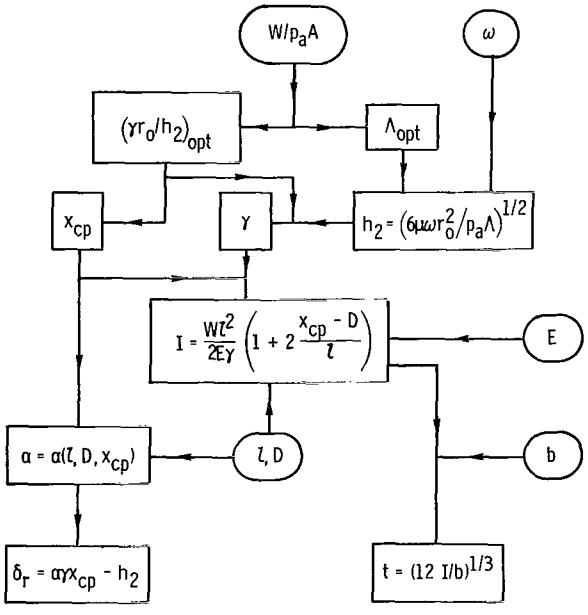

Figure 12. - Beam design procedure.

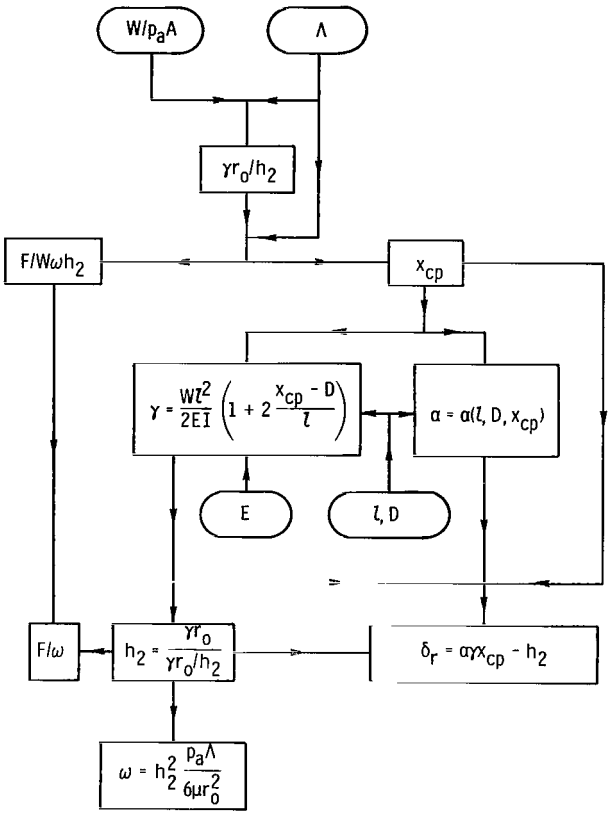

Figure 13. - Off-design calculation procedure.

"The aeronautical and space activities of the United States shall be conducted so as to contribute . . . to the expansion of human knowledge of phenomena in the atmosphere and space. The Administration shall provide for the widest practicable and appropriate dissemination of information concerning its activities and the results thereof."

—NATIONAL AERONAUTICS AND SPACE ACT OF 1958

NASA SCIENTIFIC AND TECHNICAL PUBLICATIONS

TECHNICAL REPORTS: Scientific and technical information considered important, complete, and a lasting contribution to existing knowledge.

TECHNICAL NOTES: Information less broad in scope but nevertheless of importance as a contribution to existing knowledge.

TECHNICAL MEMORANDUMS: Information receiving limited distribution because of preliminary data, security classification, or other reasons. Also includes conference proceedings with either limited or unlimited distribution.

CONTRACTOR REPORTS: Scientific and technical information generated under a NASA contract or grant and considered an important contribution to existing knowledge.

TECHNICAL TRANSLATIONS: Information published in a foreign language considered to merit NASA distribution in English.

SPECIAL PUBLICATIONS: Information derived from or of value to NASA activities. Publications include final reports of major projects, monographs, data compilations, handbooks, sourcebooks, and special bibliographies.

TECHNOLOGY UTILIZATION PUBLICATIONS: Information on technology used by NASA that may be of particular interest in commercial and other non-aerospace applications. Publications include Tech Briefs, Technology Utilization Reports and Technology Surveys.

Details on the availability of these publications may be obtained from:

SCIENTIFIC AND TECHNICAL INFORMATION OFFICE

NATIONAL AERONAUTICS AND SPACE ADMINISTRATION

Washington, D.C. 20546